AJKFLUIDS2019-5613

NUMERICAL SIMULATION OF PROPPANT TRANSPORTATION IN HYDRAULIC FRACTURE BASED ON DDPM-KTGF MODEL

Yan Zhang, Xiaobing Lu, Xuhui Zhang[1], Peng Li
Institute of Mechanics, Chinese Academy of Sciences
Beijing, China

ABSTRACT

Hydraulic fracturing is an efficient way to improve the conductivity of the tight oil or gas reservoirs. Proppant transportation in hydraulic fractures need to be investigated because the proppant distribution directly affects the oil or gas production. In this paper, the dense discrete particle model (DDPM) combined with the kinetic theory of granular flow (KTGF) are used to investigate the proppant transportation in a single fracture. In this model, the effects of proppant volume fraction, proppant-water interaction, proppant-proppant collision, and proppant size distribution are considered. The proppant-proppant collision is derived from the proppant stress tensor. This model is applicable from dilute to dense particulate flows. The simulated results are similar to the experimental data from other researchers. In further study, the two-phase flow in the cross fractures will be considered for engineering application.

Keywords: Proppant transportation, Hydraulic fracturing, Two-phase flow, DDPM-KTGF model

NOMENCLATURE

$\mathbf{u}$	velocity
α	volume fraction
P	pressure
$\boldsymbol{\tau}$	shear stress tensor
$\mathbf{g}$	gravity acceleration
D	momentum exchange coefficient
d_p	proppant diameter
C_d	drag coefficient
μ	viscosity
ρ	density
$\mathbf{F}_{KTGF}$	proppant collision force
$\mathbf{F}_{VM}$	virtual mass force
$\mathbf{F}_{PG}$	pressure gradient force
τ_r	proppant relaxation time
I_p	moment of inertia
ω_p	proppant angular velocity
C_ω	rotational drag coefficient
Θ	granular temperature
k_Θ	diffusion coefficient
γ_Θ	collision dissipation of energy
t	time

INTRODUCTION

The increase in the worldwide demand of energy causes great concern on the development of the unconventional resources such as low-permeability, shale oil and gas [1, 2]. Hydraulic fracturing is an efficient way to improve the conductivity of the tight reservoirs. First, the high pressure water is injected into the reservoirs to form cross fractures. Then, the mixture of proppant (silica sand or ceramsite) and water is pumped into the fractures to prevent their closure. The proppant distributed in the fractures forms a high permeable porous medium where the oil or gas transport efficiently.

The proppant transportation in the fractures was investigated by the physical experiments and the numerical simulation [3-6]. Li et al. [7, 8] studied the proppant movement in a single fracture and cross fractures based on the Euler-Euler two-phase flow model combined with the kinetic theory of granular flow (KTGF). Zhang et al. [9] used a couple CFD-DEM approach to model the proppant-water interaction. In this paper, the dense discrete particle model (DDPM) is used to simulate the proppant transportation in a single vertical fracture. The particle collision is described by the KTGF approach. The presented model is called DDPM-KTGF model.

In the DDPM-KTGF model, the water phase is described with an Eulerian framework while the proppant phase is treated as the discrete particles dispersed in the water. The model extends the application of the discrete particle method from dilute to dense granular flows. The effects of proppant volume fraction, proppant-water interaction, proppant-proppant collision, and proppant size distribution are taken into consideration. The interaction between the proppant and water is treated with the momentum exchange. The proppant-proppant

---

[1] Contact author: zhangxuhui@imech.ac.cn

interactions are fundamentally non-conservative unlike molecular interactions due to the dissipation of fluctuating energy from the inelastic deformation and the friction of particles with the water. Hence, the energy transport includes the kinetic transport during free flight between collision and collisional transport during collisions. This model is suitable from both dilute and dense particulate flow with different particle size distribution.

In the Section 1, the DDPM-KTGF model is introduced. Then, in the Section 2, the numerical simulation results are discussed and compared with experimental data of previous studies [4, 10]. In section 3, some future work prospects are given tentatively.

1 FORMULATION OF PROBLEM

1.1 Model Equations

1.1.1 Water Motion Equations

The water continuity equation is

$$\frac{\partial \alpha_{\mathrm{w}}}{\partial t} + \nabla \cdot \left(\alpha_{\mathrm{w}} \mathbf{u}_{\mathrm{w}} \right) = 0 \tag{1}$$

The momentum conservation equation of the water is

$$\frac{\partial \left(\alpha_{\mathrm{w}} \mathbf{u}_{\mathrm{w}} \right)}{\partial t} + \nabla \cdot \left(\alpha_{\mathrm{w}} \rho_{\mathrm{w}} \mathbf{u}_{\mathrm{w}} \mathbf{u}_{\mathrm{w}} \right) = -\alpha_{\mathrm{w}} \nabla P + \nabla \cdot \boldsymbol{\tau}_{\mathrm{w}} \tag{2}$$
$$+ \alpha_{\mathrm{w}} \rho_{\mathrm{w}} \mathbf{g} + D \left(\mathbf{u}_{\mathrm{p}} - \mathbf{u}_{\mathrm{w}} \right)$$

where $\mathbf{u}_{\mathrm{p}}$ is the proppant velocity, $\mathbf{u}_{\mathrm{w}}$ is the water velocity, α_{w} is the volume fraction of the water, P is the water pressure, ρ_{w} is the water density, $\boldsymbol{\tau}_{\mathrm{w}}$ is the water shear stress tensor, $\mathbf{g}$ is the gravity acceleration, and D is the momentum exchange coefficient.

The momentum exchange coefficient is expressed as [11]:

$$D_{\mathrm{wp}} = \begin{cases} \frac{3}{4} C_{\mathrm{D}} \dfrac{\alpha_{\mathrm{p}} \alpha_{\mathrm{w}} \rho_{\mathrm{w}} \left| \mathbf{u}_{\mathrm{w}} - \mathbf{u}_{\mathrm{p}} \right|}{d_s} \alpha_{\mathrm{w}}^{-2.65}, \alpha_{\mathrm{w}} > 0.8 \\ 150 \dfrac{\alpha_{\mathrm{p}}^2 \mu_{\mathrm{w}}}{\alpha_{\mathrm{w}} d_{\mathrm{p}}^2} + 1.75 \dfrac{\rho_{\mathrm{w}} \alpha_{\mathrm{p}} \left| \mathbf{u}_{\mathrm{w}} - \mathbf{u}_{\mathrm{p}} \right|}{d_{\mathrm{p}}}, \alpha_{\mathrm{w}} \le 0.8 \end{cases} \tag{3}$$

where α_{p} is the proppant volume fraction, which satisfies $\alpha_{\mathrm{w}} + \alpha_{\mathrm{p}} = 1$, d_{p} is the proppant diameter, and C_{d} is the drag coefficient,. The proppant volume fraction in a grid cell is calculated by dividing the total volume of the proppant by the grid cell volume.

1.1.2 Proppant Motion Equations

The proppant force balance equation is

$$\frac{d\mathbf{u}_{\mathrm{p}}}{dt} = \frac{\mathbf{u}_{\mathrm{w}} - \mathbf{u}_{\mathrm{p}}}{\tau_{\mathrm{r}}} + \frac{\mathbf{g} \left(\rho_{\mathrm{p}} - \rho_{\mathrm{w}} \right)}{\rho_{\mathrm{p}}} + \mathbf{F}_{\mathrm{KTGF}} + \mathbf{F}_{\mathrm{VM}} + \mathbf{F}_{\mathrm{PG}} \tag{4}$$

where ρ_{p} is the proppant density, $\mathbf{F}_{\mathrm{KTGF}} = -\left(\nabla \cdot \boldsymbol{\tau}_{\mathrm{p}} \right) / \alpha_{\mathrm{p}} \rho_{\mathrm{p}}$ is the proppant collision force based on proppant stress tensor given by the KTGF, $\boldsymbol{\tau}_{\mathrm{p}}$ is the proppant shear stress tensor, $\mathbf{F}_{\mathrm{VM}}$ is the virtual mass force, $\mathbf{F}_{\mathrm{PG}}$ is the pressure gradient force, which is significant when the density ratio between the water and proppant approaches unity, and τ_r is the proppant relaxation time.

The proppant torque balance equation is

$$I_{\mathrm{p}} \frac{d\boldsymbol{\omega}_{\mathrm{p}}}{dt} = \frac{\rho_{\mathrm{w}}}{2} \left(\frac{d_{\mathrm{p}}}{2} \right)^5 C_{\omega} \left(\frac{1}{2} \nabla \times \mathbf{u}_{\mathrm{w}} - \boldsymbol{\omega}_{\mathrm{p}} \right) \tag{5}$$

where I_{p} is the moment of inertia, ω_{p} is the proppant angular velocity , d_{p} is the proppant diameter, C_{ω} is the rotational drag coefficient [12].

1.1.3 Kinetic Theory of Granular Flow

The KTGF is taken to simulate the proppant collisions. Based on the KTGF approach, an additional equation, i.e. particle temperature equation, is solved to represent the fluctuations of the proppant. The fluctuations of the proppant represents the kinetic energy of the random motion of the proppant. The particle temperature equation is expressed as [13]:

$$\frac{3}{2} \left[\frac{\partial}{\partial t} \left(\rho_{\mathrm{p}} \alpha_{\mathrm{p}} \Theta_{\mathrm{p}} \right) + \nabla \cdot \left(\rho_{\mathrm{p}} \alpha_{\mathrm{p}} \mathbf{u}_{\mathrm{p}} \Theta_{\mathrm{p}} \right) \right] = \tag{6}$$
$$\left(-P_{\mathrm{p}} \mathbf{I} + \boldsymbol{\tau}_{\mathrm{p}} \right) : \nabla \mathbf{u}_{\mathrm{p}} + \nabla \cdot \left(k_{\Theta \mathrm{p}} \nabla \Theta_{\mathrm{p}} \right) - \gamma_{\Theta \mathrm{p}} + \Phi_{\mathrm{wp}}$$

where Θ_{p} is the granular temperature, P_{p} is the proppant pressure which represents the momentum exchange of particles per unit area and time, $k_{\Theta \mathrm{p}}$ is the diffusion coefficient of the granular energy, $\gamma_{\Theta \mathrm{p}}$ is the collision dissipation of energy, and Φ_{wp} is the energy exchange between the water and proppant. The details about the KTGF can be found in Li et al. [8].

1.1.4 Parcels & Particles

To simplify the computation of the proppant motion, several particles of same flow properties are put into one parcel, and then the parcel is tracked by a representative particle throughout the whole physical process. The number of particles in a parcel (N_{p}) needs to be preset, and is constant during computation. It is assumed that the velocity of the parcel is the average value of the whole particles' velocities in the parcel. The mass of the parcel is the sum of the each particle. The radius of the parcel is obtained from the mass of a parcel and the density of the parcel which is same as the particle density. In the numerical simulation, the properties of the parcels are analyzed, which is also called large "particles". Hence, the kinetic properties of the particles in a parcel are regarded as the same. The results is not sensitive to the N_{p}. It is noted that the diameter of the parcels should be less than the smallest grid size, getting rid of the convergence problems. Otherwise the volume fraction may be larger than 1. The rules on choosing the particle numbers in a parcel is based on the proppant diameter and the grid size. In

general, the diameter of the parcels is about half the size of the grid.

1.2 Initial & Boundary Conditions

The hydraulic fractures are always cross fractures with several primary fractures and many subsidiary fractures. Firstly, the DDPM-KTGF model is validated in simulating the proppant transportation in fractures. A single vertical fracture is used simplicity (Fig. 1). It is assumed that the height and width of the fracture remain constant in the proppant transportation. The length × height × width of the fracture is 380mm × 76mm × 2mm. The field is divided into hexahedral structured cells for both the computation accuracy and convergence. Initially, the fracture is filled with water without proppant. The left is set as a velocity inlet and the right is set a pressure outlet (0 gauge pressure). The proppant is not allowed to leave the fracture. Inner walls is set as no-slip wall boundary condition. The parameters adopted in the numerical simulation are listed in Table 1.
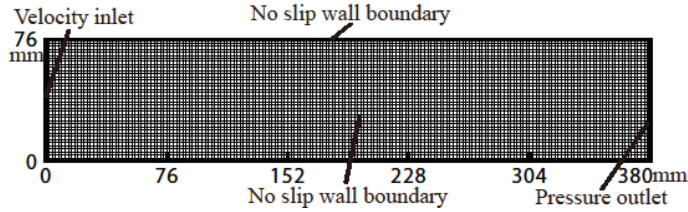
FIGURE 1: A SINGLE VERTICAL FRACTURE

TABLE 1: PARAMETERS USED IN NUMERICAL SIMULATION

Parameters	Case 1	Case 2	Case 3
Fracture size: length, height, width(mm)	380, 76, 2	380, 76, 2	380, 76, 2
Grid size: length, height, width(mm)	2, 2, 2	2, 2, 2	2, 2, 2
Grid number	7220	7220	7220
Proppant density(kg/m^3)	2650	2650	2650
Proppant diameter(mm)	0.6	0.6	0.6
Water density(kg/m^3)	1000	1000	1000
Water viscosity(Pa·s)	0.001	0.001	0.001
Inlet velocity(m/s)	0.1	0.2	0.3
Particle numbers in a parcel	5	5	5

1.3 Solution Algorithms

The phase-coupled SIMPLE method is adopted to solve the water motion equations. The Green-Gauss node based method is used for the gradient discretization. The QUICK scheme is used for the solution of the volume fraction equation. The momentum equation is discretized with second order upwind scheme. The first order implicit schemes are used for the temporal discretization.

As the trajectory of the proppant is computed, the effects of the proppant will be incorporated in the subsequent water phase calculations, such as the momentum exchange term in Eq.(2). The proppant variables, such as the density, and velocity, are mapped to the Eulerian framework to compute the water-proppant interaction. Generally, the effects of the proppant are only applied to the grid cell that contains the proppant. In this paper, a grid node averaging method is used to distribution the proppant effects to neighbouring grid nodes. It reduces the grid dependency of DDPM simulations. The variables of the proppant is averaged by the following equation:

$$\overline{\varphi}_{node} = \sum_k f\left(\mathbf{x}_p^k - \mathbf{x}_{node}\right)\varphi_p \tag{7}$$

where φ_p is the proppant variable, $\overline{\varphi}_{node}$ is the accumulation of the proppant variable on the node for all the proppant k, f is a weighting function, $\mathbf{x}_p^k$ is the proppant position, and $\mathbf{x}_{node}$ is the node position. The Gaussian weighing function is used and expressed as:

$$f\left(\mathbf{x}_p^k - \mathbf{x}_{node}\right) = \left(\frac{1}{\pi}\right)^{\frac{3}{2}} \exp\left(-\frac{\left|\mathbf{x}_p^k - \mathbf{x}_{node}\right|^2}{\Delta x^2}\right) \tag{8}$$

where Δx is a characteristic length of the grid cell.

2 RESULTS & DISCUSSION

Figure 2 shows the comparison of the proppant distribution in the fracture between the simulated results and experimental data [4] at the time of 20s. The inlet velocity of the proppant is 0.1 m/s, 0.2 m/s, and 0.3 m/s, respectively. The experimental apparatus of the Tong and Mohanty [4] consisted of one primary fracture and one secondary fracture. In this paper, the proppant distribution in the primary fracture is compared. In Fig. 2, the proppant distribution is basically the same, the distance between the initial proppant bed front and the inlet increases with the increase of the inlet velocity. Figure 3 gives the comparison of the equilibrium height. The equilibrium height decreases with the increase of the inlet velocity and more proppant moves further in the fracture, because the carrying capacity of the water is greater at higher inlet velocity. It can be found that the simulated equilibrium height is slightly larger than the experiment data. This is because there is a secondary fracture in the experiment apparatus. Some proppant move into the secondary fracture. The comparison verifies the DDPM-KTGF model in the analysis on the proppant transportation in the fractures.
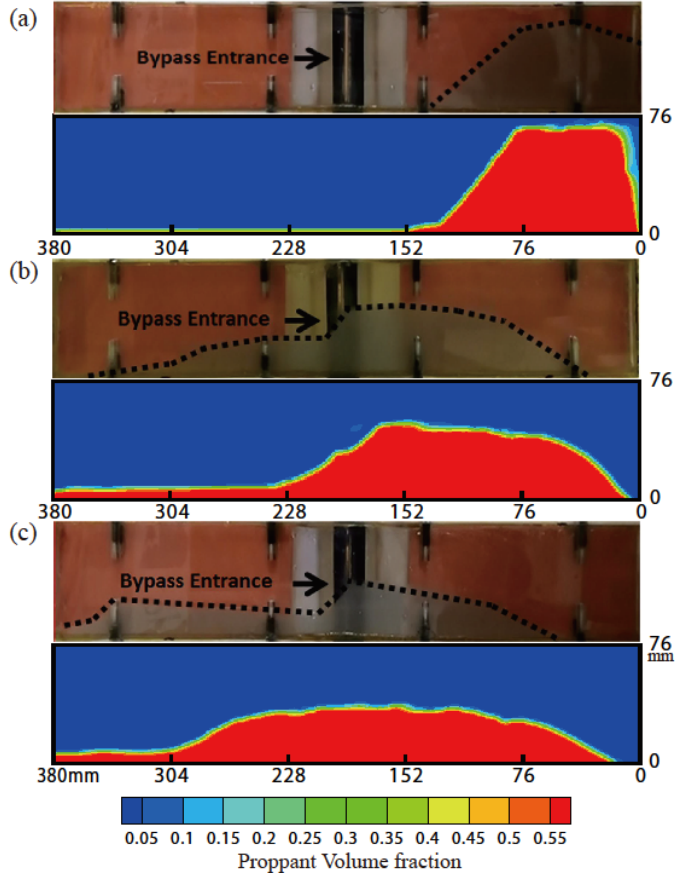
FIGURE 2: THE COMPARISON OF THE PROPPANT DISTRIBUTION IN THE FRACTURE BETWEEN THE SIMULATION RESULTS AND EXPERIMENTAL DATA [4] AT TIME OF 20s. THE INLET VELOCITY OF THE PROPPANT IS (a) 0.1 m/s, (b) 0.2 m/s, AND (c) 0.3 m/s.
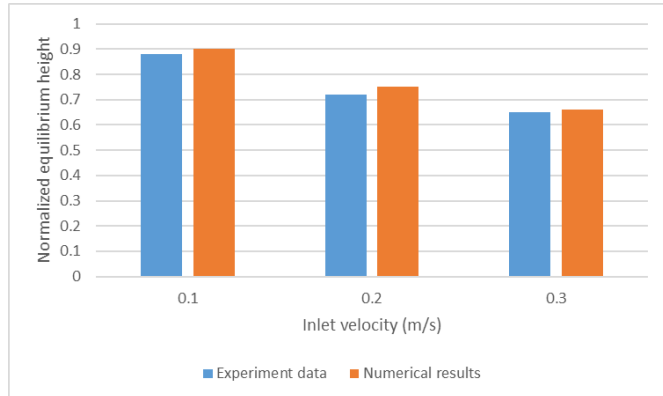

FIGURE 3: THE COMPARISON OF THE EQUILIBRIUM HEIGHT

The proppant quickly settles to the bottom of the fractures after entering into the fractures due to the self-gravity and the low viscosity of the water, and then form a proppant bed. The proppant bed will not be moved by the subsequent pumped mixture (proppant and water). The height of the proppant bed gradually grows and the flow cross section available for the mixture reduces. Consequently, both the mixture's flow velocity and the water's carrying capacity increase. The height of the proppant bed will be in an equilibrium status, which is called equilibrium proppant height. After the equilibrium proppant height is reached, the proppant bed moves far in the fractures under constant the height. Figure 4 gives the formation process of the proppant bed based on simulated results. It is similar to the experimental results of Alotaibi and Miskimins [10].
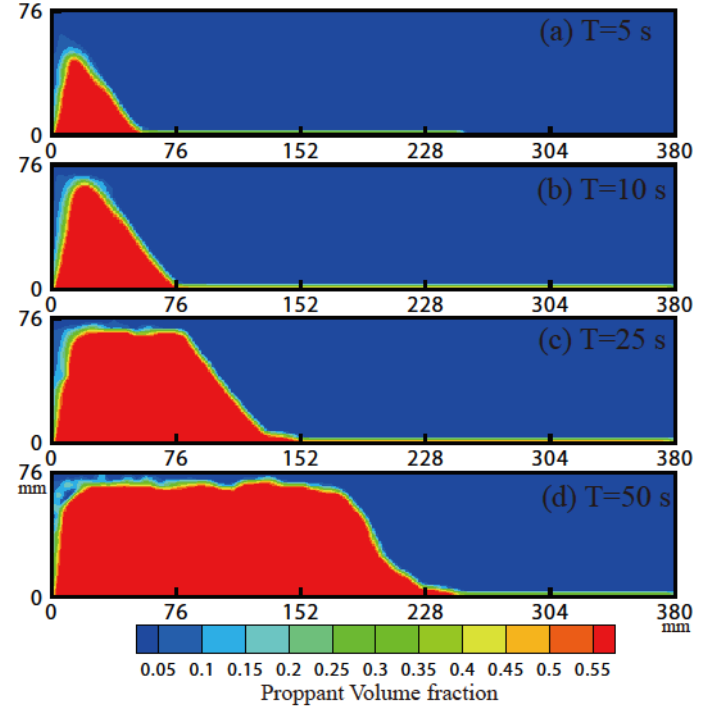

FIGURE 4: THE FORMATION PROCESS OF THE PROPPANT BED: (a) 5 s, (b) 10 s, (c) 25 s, (d) 50 s

Figure 5(a) shows the proppant movement time in the fracture. The early pumped proppant form the initial proppant bed and will stop moving. The subsequent pumped proppant flow over the bed surface and settles at the front of the bed. It affects the formation of the proppant bed. Figure 5(b) gives the proppant velocity. The velocity of the particles in the bed is almost zero while is very large above the bed surface due to the increase of the water velocity.
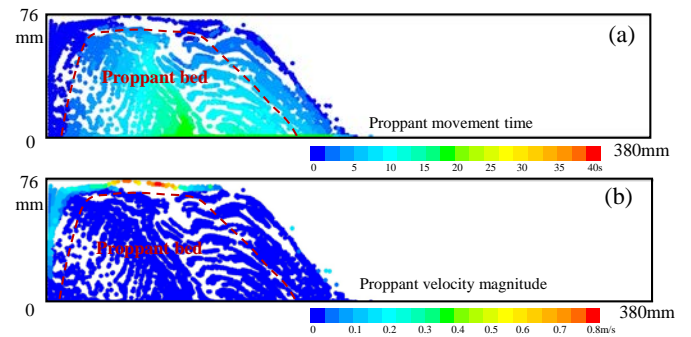
FIGURE 5: (a) PROPPANT MOVEMENT TIME, (b) PROPPANT VELOCITY MAGNITUDE

3 FUTURE WORK PROSPECTS

In this paper, the DDPM-KTGF model and the problem of the proppant transportation in a single vertical fracture are present. In the future work, the proppant transportation in complex fractures will be considered. The critical condition for proppant deposition in the fractures and the mechanism of proppant from a primary fracture into the subsidiary fractures will be obtained. In addition, some improvement of the DDPM-KTGF model can be made. For example, the rough wall model [14] can be used to capture more realistic behavior of the proppant interaction with the fracture wall.

CONCLUSION

The DDPM-KTGF model is introduced in this paper. The proppant transportation in a single vertical fracture is studied based on this model.

From simulated results, the proppant quickly settles to the bottom and form a proppant bed after entering the fracture. The proppant bed will increase the water and proppant velocity due to the decrease of the flow cross section. The simulated results are similar to other researchers' experimental data.

This model can analyze the proppant transportation in given fracture geometries, while more efforts should be made to model the coupling process of the development of fractures and the proppant transportation.

ACKNOWLEDGEMENTS

REFERENCES

[1] Zeng, Q.L., Wang, T., Liu, Z.L., Zhuang, Z., 2017. Simulation-Based Unitary Fracking Condition and Multiscale Self-Consistent Fracture Network Formation in Shale. ASME Journal of Applied Mechanics, Vol. 84, pp.051004.1-7.

[2] Wang, J., Elsworth, D., 2018. Role of proppant distribution on the evolution of hydraulic fracture conductivity. Journal of Petroleum Science and Engineering, Vol. 166, pp. 249-262.

[3] Sahai, R., Miskimins, J., E. Olson, K., 2014. Laboratory Results of Proppant Transport in Complex Fracture Systems, SPE Hydraulic Fracturing Technology Conference, The Woodlands, Texas, USA.

[4] Tong, S., Mohanty, K.K., 2016. Proppant transport study in fractures with intersections. Fuel, Vol. 181, pp. 463-477.

[5] Wang, J., Elsworth, D., 2018. Role of proppant distribution on the evolution of hydraulic fracture conductivity. Journal of Petroleum Science and Engineering, Vol. 166, pp. 249-262.

[6] Chang, O., Kinzel, M., Dilmore, R., Wang, Y.L., 2018. Physics of Proppant Transport Through Hydraulic Fracture Network. ASME Journal of Energy Resources Technology, Vol. 140, pp.032912.1-11

[7] Li, P., Su, J.Z., Zhang, Y., Zhang, X.H., Lu, X.B., 2017. The two phase flow of proppant-laden fluid in a single fracture. Mechanics in Engineering, Vol. 39, pp. 135-144.

[8] Li, P., Zhang, X.H., Lu, X.B., 2018. Numerical simulation on solid-liquid two-phase flow in cross fractures. Chemical Engineering Science, Vol. 181, pp. 1-18.

[9] Zhang, G., Gutierrez, M., Li, M., 2017. A coupled CFD-DEM approach to model particle-fluid mixture transport between two parallel plates to improve understanding of proppant micromechanics in hydraulic fractures. Powder Technology, Vol. 308, pp. 235-248.

[10] Alotaibi, M., Miskimins, J., 2015. Slickwater Proppant Transport in Complex Fractures: New Experimental Findings & Scalable Correlation, SPE Annual Technical Conference and Exhibition, Houston, Texas, USA.

[11] Gidaspow, D., 1994. Multiphase Flow and Fluidization: Continuum and Kinetic Theory Descriptions. Academic Press, Boston.

[12] Dennis, S.C.R., Singh, S., Ingham, D.B., 1980. The steady flow due to a rotating sphere at low and moderate Reynolds numbers. Journal of Fluid Mechanics, Vol. 101, pp. 257-279.

[13] Ding, J., Gidaspow, D., 1990. A bubbling fluidization model using kinetic theory of granular flow. AIChE Journal, Vol. 36, pp. 523-538.

[14] Sommerfeld, M., Huber, N., 1999. Experimental analysis and modelling of particle-wall collisions. International Journal of Multiphase Flow, Vol. 25, pp.1457-1489.